Advanced Materials **21**, 3644-3648 (2009)

DOI: 10.1002/adma.200803850

Madelung Strain in Cuprate Superconductors – A Route to Enhancement of the Critical Temperature

By *Vladimir Y. Butko*, *Gennady Logvenov*, *Natasha Bozovic*, *Zoran Radovic* and *Ivan Bozovic*[*]

[*] Dr. Ivan Bozovic (Corresponding-Author), Dr. Gennady Logvenov
Department of Condensed Matter Physics and Materials Science
Brookhaven National Laboratory
Upton NY 11973, USA
e-mail: bozovic@bnl.gov

Dr. Vladimir Butko,
Department of Condensed Matter Physics and Materials Science
Brookhaven National Laboratory
Upton NY 11973, USA
and
Ioffe Physical Technical Institute
26 Polytechnical street
St. Petersburg 194021, Russia.

Prof. Natasha Bozovic
Department of Mathematics
San Jose State University
San Jose, California 95192, USA

Prof. Zoran Radovic
Department of Physics
University of Belgrade
Belgrade 11000, Serbia

Interfaces between complex oxides display exciting phenomena - high-mobility electron gas,[1] quantum Hall effect,[2] magnetism,[3] quantum oscillations,[4] and superconductivity.[5-7] Despite a very intense study, some puzzling questions remain. The superconducting critical temperature (T_c) in cuprate films consisting of a metal (M) and an insulator (I) layers depends, surprisingly, on the deposition sequence: $T_c \approx 15$ K in I-M while $T_c \approx 30$ K in M-I structures.[7] If one or both layers are superconducting (S) with $T_c \approx$ 35-40 K, interfacial layer shows enhanced superconductivity[6,7] with $T_c > 50$ K. In this contribution, we resolve these puzzles by pinpointing the structural origin of the I-M vs. M-I asymmetry and of the interfacial enhancement: T_c scales linearly with the c_0 lattice constant, and the volume of unit cell of the top layer unexpectedly adjusts to that of the bottom layer. The later is caused by long-range electrostatic interactions, and by engineering this 'Madelung Strain' we can fabricate crystals with otherwise unattainable structural parameters and electronic properties.

For film synthesis we employed a unique atomic layer-by-layer molecular beam epitaxy system equipped with advanced tools for in-situ surface analysis including reflection high energy electron diffraction and time-of-flight ion scattering spectroscopy.[6-8] Using this technique we reproducibly fabricate single-crystal films with atomically smooth surfaces and interfaces; the typical surface roughness estimated from atomic-force microscope images is

0.2-0.5 nm. For this study we deposited a number of single-phase and bilayer films, using as the constituent materials La_2CuO_4, an antiferromagnetic insulator (I in what follows) and $La_{1.56}Sr_{0.44}CuO_4$, a non-superconducting metal (M). The films were grown on single-crystal $LaSrAlO_4$ (LSAO) substrates polished with the surface perpendicular to the (001) crystallographic direction. Depending on the deposition sequence we will denote the bilayers by M-I or I-M, where the first letter identifies the 'bottom' layer (i.e., the one next to the substrate) and the second letter refers to the top layer. We have annealed some of the films ex situ in ozone for 20-40' at 150-250^{0}C; this procedure[6] leaves M layers essentially unaffected while in I layers it introduces interstitial oxygen thereby forming $La_2CuO_{4+\delta}$, a superconductor (S) with typical $T_c \approx 35$ K. Transport measurements on these bilayers showed results consistent with Ref. 6, i.e., $T_c \approx 15$ K in I-M, $T_c \approx 30$-35 K in M-I, and $T_c \approx 50$ K in M-S structures.

The lattice parameters of single-phase and bilayer films were determined by high-resolution X-ray diffraction. Typical out-of plane diffractograms for high scanning angles are shown in **Figure 1a** for M-I and in **Figure 1b** for I-M bilayers. Since the c-axis lattice parameters of the constituent materials are fairly different, $c_0 \approx 13.15$ Å for I and $c_0 \approx 13.25$ Å for M, one would expect to see in both I-M and M-I bilayers pairs of close but distinct Bragg peaks. This is illustrated in **Figure 1c** and **Figure 1d** where we show the bilayer diffractograms calculated assuming that the constituent layers maintained their original crystallographic structure. However, as seen from **Figures1 a-d**, no such splitting of the Bragg peaks is observed even at high scanning angles. This is the central experimental finding of the present paper: surprisingly, each bilayer shows a single value of the out-of plane lattice parameter. Adjustment of the in-plane lattice constants of the film to those of the substrate, i.e., pseudomorphic growth, is not surprising as long as the film is thinner than the critical thickness. However, as seen from Table 1, the volume of unit cell for M is noticeably different from that of I, and in view of the small compressibility one would expect that the out-of-plane lattice constants would carry over that difference.

More can be learned by comparing bilayers to single-phase films, see **Table 1**. In I-M structures $c_0 = 13.169$ Å, rather close to (within 0.1 % of) that in single-phase I films, $c_0 = 13.154$ Å, while in M-I bilayers it is almost identical to that in single-phase M films, $c_0 = 13.245$ Å. In both cases the c_0 lattice constant and the unit cell volume of the top layer essentially adjust to those of the bottom layer. This is illustrated graphically in **Figure 2a**, which shows that the diffractograms of I-M and M-I are clearly different, while **Figure 2b** shows that M-I looks basically the same as M, and **Figure 2c** shows I-M being identical to I. The detected lattice distortions are large – e.g., in I-M bilayers the contraction of c_0 in M reaches ~ 0.08 Å, comparable to the effect of a high pressure[9,10] of about 2 GPa. If an M-I bilayer is annealed in ozone - the procedure which is known[6] to introduce interstitial oxygen in I while leaving M essentially unaffected - we find that surprisingly both layers expand. The out-of-plane lattice constant in such M-S bilayers is $c_0 = 13.289$ Å, perceptibly longer then in single-phase M films, but again there is no apparent splitting of the Bragg peaks and the unit-cell volumes of the two constituent layers stay equal.

In-plane lattice constant values indicate that 20 unit cells thick I layers are relaxed, i.e. both a_0 and b_0 lattice constants are close to their bulk values,[11,12] while M layers of the same thickness are pseudomorphic. This can be understood by recalling that the critical thickness for I on $LaSrAlO_4$ is less then 20 lattice constants[13,14] while for M it should be significantly larger because of its much better lattice match to the substrate. [The mismatch between in-plane lattice constants of an I film and a $LaSrAlO_4$ substrate is -1.1 %, compressive, while between M and $LaSrAlO_4$ it is just +0.03 %, tensile.] On the other hand, the large adjustments

of c_0 lattice constants and unit-cell volumes of the top I and M layers is surprising and this finding requires a more thorough analysis that is presented later in the paper.

Our next key observation is illustrated in **Figure 3** where we show the values of T_c in our single-phase films and bilayers as a function of the c_0 lattice constant. Apparently, the scaling of T_c with c_0 is almost perfectly linear. This finding allows us to link, in a phenomenological way, the observed 'asymmetry' between the superconducting properties of I-M and M-I bilayers to their significant and unexpected structural differences, and the enhanced T_c in M-S bilayers to the anomalous elongation along the c-axis. M-S bilayers have the longest c_0 = 13.289 Å and correspondingly the highest $T_c \approx 50$ K, which is ~ 40% higher than in single-phase S films prepared under identical conditions and ~ 20% larger than T_c in optimally doped $La_{2-x}Sr_xCuO_4$ bulk crystals. We note that roughly linear dependence of T_c on c_0 has already been noticed[14-18] in $La_{2-x}Sr_xCuO_4$ samples with different level of Sr doping; however, note that there is no Sr substitution here - the lattice stretches for a different cause, and further out.

The observed adjustment of the unit cell volume in bilayers can be understood qualitatively using a simple ionic model. The cohesion energy of ionic crystals can be approximated as:

$$U = \frac{e^2}{2}\sum \frac{q_i q_j}{\left|r_i - r_j\right|} + \frac{1}{2}\sum A_{ij}\exp\left(-B_{ij}\left|r_i - r_j\right|\right) \qquad (1)$$

where the first term is the Madelung energy, $\boldsymbol{r_i}$ and $\boldsymbol{r_j}$ are the positions of the ions, q_i and q_j are their charges (in units of e), the second term is the core repulsion energy in the standard Born-Mayer form, and the sums are over all i, j with $\boldsymbol{r_i} \neq \boldsymbol{r_j}$. The contributions from Van der Waals interactions, covalency, etc., are small (less than 1 %) and included implicitly through the choice of coefficients A_{ij} and B_{ij}. Here we have used the following Born-Mayer parameters: $A_{Cu\text{-}O}$ = 0.302 keV, $A_{La\text{-}O}$ = 1.181 keV, $A_{O\text{-}O}$ = 0.288 keV and $B_{Cu\text{-}O} = B_{La\text{-}O} = B_{O\text{-}O} = 2.66$ Å^{-1}, which reproduce accurately the crystal structure[11] of La_2CuO_4 as well its bulk modulus.[12] Sr doping is modeled as the simple change in ionic charges q_i (for the details see Ref. 19). This simple approach has been demonstrated to account well for the cohesion energy, the charge-transfer gap, the phonon frequencies, and the structural changes induced by chemical- and photo-doping.[19,20]

To investigate whether the structure of the top layer can be influenced by the bottom layer, we have performed simulations on LSAO-I, M-I and I-M bilayers in which we kept the bottom layer frozen in its experimental configuration, calculated the crystal energy of the bilayer by summation over both layers, and varied the structure of the top layer until we recahed the minimum-energy configuration. The results came very close to the experimental observations: we calculate that in I-M bilayers the value of c_0 should be very close to (0.1 % longer than) the one found in a single-phase I film, while in M-I bilayers it should be close to (0.3 % shorter then) that of M.

Thus, our numerical simulations suggest that the observed variation of the out-of-plane lattice constant of the top layer originates largely from the contribution to Madelung energy that comes from the Coulomb interaction between that layer and the substrate or the buffer layer. We propose to call this phenomenon the 'Madelung Strain'. A very clear manifestation of the presence of Madelung strain is the fact that the critical thickness of I grown directly on LSAO is less than 20 nm while it is apparently much larger for an I layer grown on an M buffer, even though the in-plane lattice constants of M and LSAO are virtually identical. This implies that long-range Coulomb interaction along the c-axis between the ionic compounds I

and LSAO contributes to the crystal energy in I, while the metallic M buffer screens this interaction and decouples I from LSAO.

Observation of Madelung strain in cuprate bilayers demonstrates, in a rather explicit way, the importance of out-of-plane Coulomb interactions. The recent observation of colossal photo-induced expansion[19,20] also indicated that in cuprates mobile charge excitations are strongly coupled to ionic displacements along the c-axis. The results presented here and further studies of Madelung strain and screening in epitaxial multi-layers can impact theoretical understanding of the mechanism of HTS and of the relationship between electronic properties and structure in other ionic crystals of interest.

We have elucidated the observed peculiarities in superconducting properties of I-M, M-I and M-S bilayers by discovering their structural origin, but this explanation leaves two important questions open. The first is why T_c scales with c_0 to begin with. One possibility is that this is related to the change in the position of apical oxygen which may play an important role[21-26] in controlling T_c. Other mechanism of T_c enhancement in cuprate bilayers have been proposed as well.[27,28] Resolving this question may be tantamount to deciphering the mechanism of HTS which is beyond the scope of this paper; nevertheless, the fact that the key superconductive property, T_c, increases linearly with c_0 is notable both as a hint to theorists and as a guideline in search for better superconductors. It seems worth trying to further increase c_0 while maintaining the optimum doping level and without increasing disorder; modifying the Madelung strain - e.g. by choosing different ionic compounds for the substrate and/or the bufffer layer - is one possible approach. The second puzzle is why the top layer always adjusts to the bottom one and not the other way round. Here, we can only note that our bilayers are metastable structures - if we heat a bilayer until it melts and then cool it back until it recrystallizes we will not recover the same bilayer but rather obtain a single-phase film doped uniformly by Sr. Our film synthesis is at least partly controlled by the kinetics; impinging atoms ionize, move on the surface, and eventually embed themselves into a metastable crystal lattice that is influenced by the solid structure underneath and by the long-range Coulomb forces emanating from it.

In conclusion, we have identified the structural origin of the I-M vs. M-I asymmetry and of the interfacial enhancement of superconductivity observed in cuprate bilayers. The volume of unit cell of the top layer adjusts to that of the bottom layer, under the influence of long-range electrostatic interactions. Numerical simulations suggest that this Madelung strain can be manipulated by varying the substrate and/or the composition and the thickness of buffer layer. This provides a new method of fabrication of crystals with extraordinary physical properties arising from unusual structural parameters that cannot be attained otherwise, even by applying large hydrostatic or uniaxial pressure.

Experimental

Epitaxial film growth. The samples studied in this work were synthesized using an advanced oxide molecular-beam epitaxy (MBE) system at Brookhaven National Laboratory. This system has 16 pneumatically shuttered metal atom sources, a pure ozone gas source, a scanning quartz-crystal monitor, a 16-channel atomic absorption spectroscopy system for measuring the deposition rates in real time, a reflection high-energy electron diffraction (RHEED) system, and a time-of-flight ion scattering and recoil spectroscopy (TOF-ISARS) system.[8] This technique enables reproducible fabrication of atomically smooth films of cuprate superconductors and other related complex oxides. Atomic-layer-by-layer synthesis allows for digital control of film thickness and fabrication of various hetero-structures.[6-8]

Here, we have used as building blocks three cuprates, an insulator La_2CuO_4 (I), an overdoped and non-superconducting metal $La_{1.56}Sr_{0.44}CuO_4$ (M), and oxygen-doped, superconducting $La_2CuO_{4+\delta}$ (S). All the blocks were 20 unit cells (UC) thick unless indicated otherwise. The films were grown on single-crystal $LaSrAlO_4$ (LSAO) substrates, 10x10x1 mm^3 in size and polished with the surface perpendicular to the (001) direction. During growth, the substrate temperature was kept at 650^0C (nominal pyrometer reading) and the chamber pressure at $6*10^{-6}$ Torr of ozone. The films that contain I layers were all cooled down in high vacuum (with the ozone source shut off); to ensure removal of residual interstitial oxygen they were also post-annealed ex-situ in high vacuum for extended periods (30-120') until saturation, i.e., until subsequent annealing had no effect on measured transport properties. The films that contain S layers were either cooled down in ozone and/or post-annealed in ozone (ca. 10 Torr) for extended periods (20-60') at $T = 200\text{-}350^0$C.

Film characterization. The films were characterized in situ by RHEED and ex situ by Atomic force microscopy (AFM), X-ray diffraction (XRD), and transport (electric resistance and magnetic susceptibility) measurements. AFM showed atomically smooth surfaces; typical root-mean-square surface roughness was 0.2-0.5 nm, less than the unit cell (UC) thickness, which in $La_{2-x}Sr_xCuO_{4+\delta}$ is about 1.3 nm. High-resolution X-ray diffraction was measured using an X-pert PRO PANalytical 4-circle diffractometer with a Cu tube as the X-ray radiation source. For the incident beam optics we used a hybrid monochromator consisting of a parabolic mirror and a 4-bounce Bartels monochromator that contains two (220)-cut Ge monocrystals) and provides resolution better than 19 arcsec. The detector optics side contained an X-ray proportional detector and a 1mm-wide slit or alternatively a triple-axis monochromator with a hybrid 0.5^0 slit. The high quality of films was evident from rocking curves around (002) peak that showed the full-width-at-half-maximum as low as 0.03º-0.06º, indicating a very narrow mosaic spread. The observation of finite-thickness oscillations in X-ray reflectance spectra was also indicative of atomically smooth films and consistent with the atomic-force microscopy data. In-plane and out-of plane lattice parameters were determined using the Nelson-Riley algorithm [29] from a series of Bragg peaks observed in 2θ-ω scans.

Acknowledgements

We benefited from useful comments and suggestions by A. Gozar, D. Savage, A. Millis, N. Ashcroft, M. L. Cohen, T. H. Geballe, O. Pelleg, C. Di Castro, W. Hardy, D. Khomskii, M. Naito, V. Kresin, M. Lagally, A. Alexandrov, F. Kusmartsev, P. Abbamonte and A. Balatsky. The work at BNL was supported by US DOE contract MA-509-MACA. (Supporting Information is available online from Wiley InterScience or from the authors.)

[1] A. Ohtomo and H. Y. Hwang, *Nature* **2004**, *427*, 423-426.

[2] A. Tsukazaki, A. Ohtomo, A. T. Kita, Y. Ohno, H. Ohno and M. Kawasaki, *Science* **2007**, *315*, 1388-1391.

[3] A. Brinkman, M. Huijben, M. Van Zalk, J. Huijben, U. Zeitler, J. C. Maan, W. G. van der Wiel, G. Rijnders, D. H. A. Blank and H. Hilgenkamp, *Nat. Mater.* **2007**, *6*, 493-496.

[4] M. van Zalk, J. Huijben, A. J. M. Giesbers, M. Huijben, U. Zeitler, J. C. Maan, W. G. van der Wiel, G. Rijnders, D. H. A. Blank, H. Hilgenkamp and A. Brinkman, arXiv:0806.4450.

[5] N. Reyren, S. Thiel, A. D. Caviglia, L. F. Kourkoutis, G. Hammerl, C. Richter, C. W. Schneider, T. Kopp, A. S. Ruetschi, D. Jaccard, M. Gabay, D. A. Muller, J.-M. Triscone and J. Mannhart, *Science* **2007**, *317*, 1196-1199.

[6] I. Bozovic, G. Logvenov, I. Belca, B. Narimbetov and I. Sveklo, *Phys. Rev. Lett.* **2002**, *89*, 107001.

[7] A. Gozar, G. Logvenov, L. Fitting Kourkoutis, A. T. Bollinger, L. A. Giannuzzi, D. A. Muller and I. Bozovic, Nature **2008**, *455*, 782-5.

[8] I. Bozovic, *IEEE Trans. Appl. Supercond.* **2001**, *11*, 2686-2695.

[9] J. Shu, J. Akella, J. Z. Liu, H. K. Mao and L. W. Finger, *Physica C* **1991**, *176*, 503-506.

[10] N. C. Hyatt, J. A. Hriljac, Y. Miyazaki, I. Gameson and P. P. Edwards, *Phys. Rev. B* **2002**, *65*, 014507.

[11] P. G. Radaelli, D. G. Hinks, A. W. Mitchell, B. A. Hunter, J. L. Wagner, B. Dabrowski, K. G. Vandervoort, H. K. Viswanathan and J. D. Jorgensen, *Phys. Rev. B* **1994**, *49*, 4163-4175.

[12] A. Migliori, W. M. Visscher, S. E. Brown, Z. Fisk, S.-W. Cheong, B. Alten, E. T. Ahrens, K. A. Kubat-Martin, J. D. Maynard, Y. Huang, D. R. Kirk, K. A. Gillis, H. K. Kim and M. H. W. Chan, *Phys. Rev. B* **1990**, *41*, 2098-2102.

[13] C. Cancellieri, Ph.D. Thesis, EPFL (2008) http://library.epfl.ch/theses/?nr=4120

[14] J.-P. Locquet, J. Perret, J. Fompeyrine and E. Machler, *Nature* **1998**, *394*, 453-456.

[15] H. Sato and M. Naito, *Physica C* **1997**, *274*, 221-226.

[16] F. Gugenberger, C. Meingast, G. Roth, K. Grube, V. Breit, T. Weber, H. Wühl, S. Uchida and Y. Nakamura, *Phys. Rev. B* **1994**, *49*, 13137-13142.

[17] J.-P. Locquet, J. Perret, J. W. Seo and J. Fomperyrine, in "*Superconducting and related oxides: Physics and Nanoengineering III*", D. Pavuna and I. Bozovic, editors, SPIE Proceedings **3481** (SPIE, Bellingham, 1998) pp. 248-264.

[18] H. Sato, M. Naito, A. Tsukada, S. Karimoto and A. Matsuda, *Physica C* **2001**, *362*, 186-194.

[19] Z. Radovic, N. Bozovic and I. Bozovic, *Phys. Rev. B* **2008**, *77*, 092508.

[20] N. Gedik, D. S. Yang, G. Logvenov, I. Bozovic and A. H. Zewail, *Science* **2007**, *316*, 425-429.

[21] A. A. R. Fernandes, J. Santamaria, S. L. Bud'ko, O. Nakamura, J. Guimpel and I. K. Schuller, *Phys. Rev. B* **1991**, *44*, 7601-7606.

[22] Y. Ohta, T. Tohyama and S. Maekawa, *Phys. Rev. B* **1991**, *43*, 2968-2982.

[23] L. F. Feiner, M. Grilli and C. Di Castro, *Phys. Rev. B* **1992**, *45*, 10647-10669.

[24] C. Lubritto, K. Rosciszewski and A. M. Oles, *J. Phys.: Condens. Matter*. **1996**, *8*, 11053-11068.

[25] E. Pavarini, I. Dasgupta, T. Saha-Dasgupta, O. Jepsen and O. K. Andersen, *Phys. Rev. Lett.* **2001**, *87*, 047003.

[26] J. A. Slezak, Jinho Lee, M. Wang, K. McElroy, K. Fujita, B. M. Andersen, P. J. Hirschfeld, H. Eisaki, S. Uchida and J. C. Davis, *Proc. Nat. Acad. Sci.* **2008**, *105*, 3203-3207.

[27] S. A. Kivelson, *Physica B* **2002**, *318*, 61-67.

[28] S. Okamoto and T. A. Maier, *Phys. Rev. Lett.* **2008**, *101*, 156401.

[29] H. Lipson and H. Steeple, *Interpretation of X-ray Powder Diffraction Patterns* (Macmillan, London, 1970).

[30] J. D. Jorgensen, B. Dabrowski, Shiyou Pei, D. G. Hinks, L. Soderholm, B. Morosin, J. E. Schirber, E. L. Venturini and D. S. Ginley, *Phys. Rev. B* **1988**, *38*, 11337-11345.

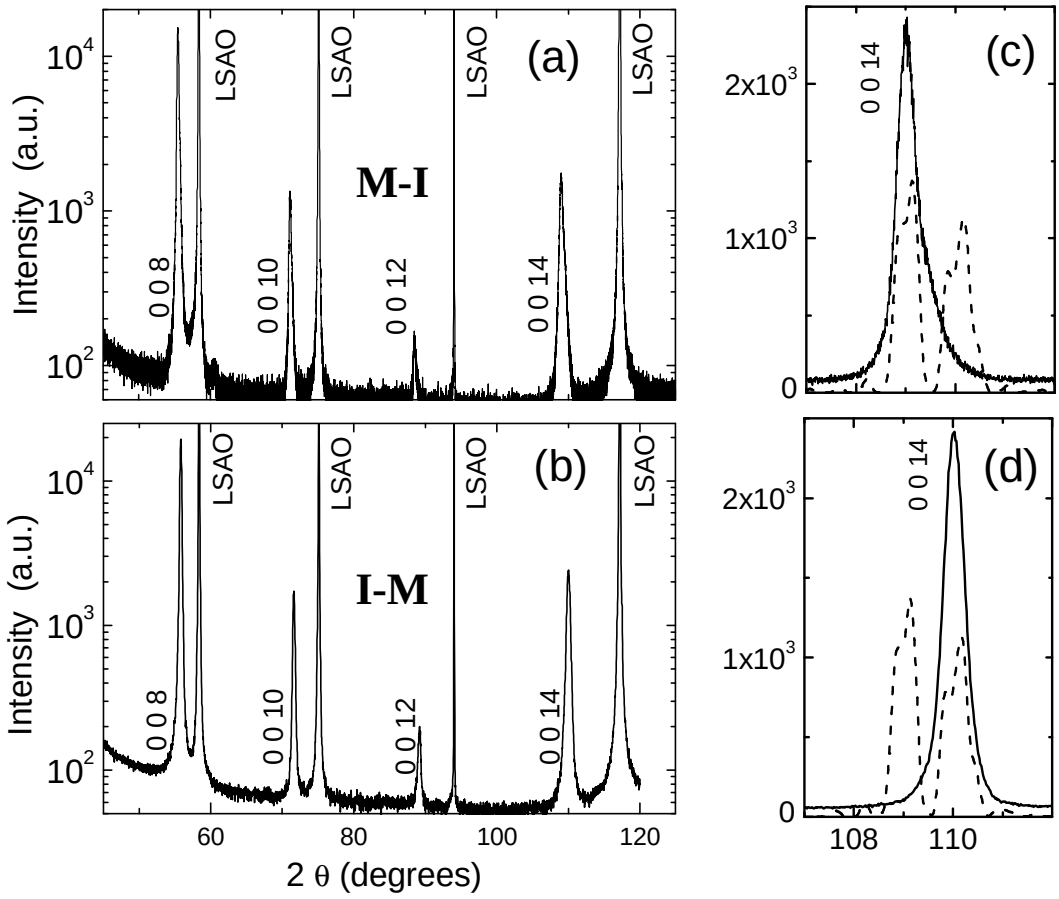

Figure 1. In bilayers, X-ray diffraction shows that the two constituent layers have assumed the same crystal structure. (a) ω-2θ scan from an M-I bilayer grown on LSAO substrate, and (b) the same for an I-M bilayer. The symbols I, M, and LSAO are defined in the caption to Table I. Each constituent layer is 20 unit cells (26 nm) thick and oriented with CuO_2 planes parallel to the surface. (c) The measured diffractograms (solid lines) of an M-I bilayer compared with simulation in which M and I layers retain their bulk (single layer) structure, and (d) the same for an I-M bilayer. Experimentally, every bilayer shows a single value of the c_0 lattice constant. The same is actually true for the other two lattice constants, a_0 and b_0, as well.

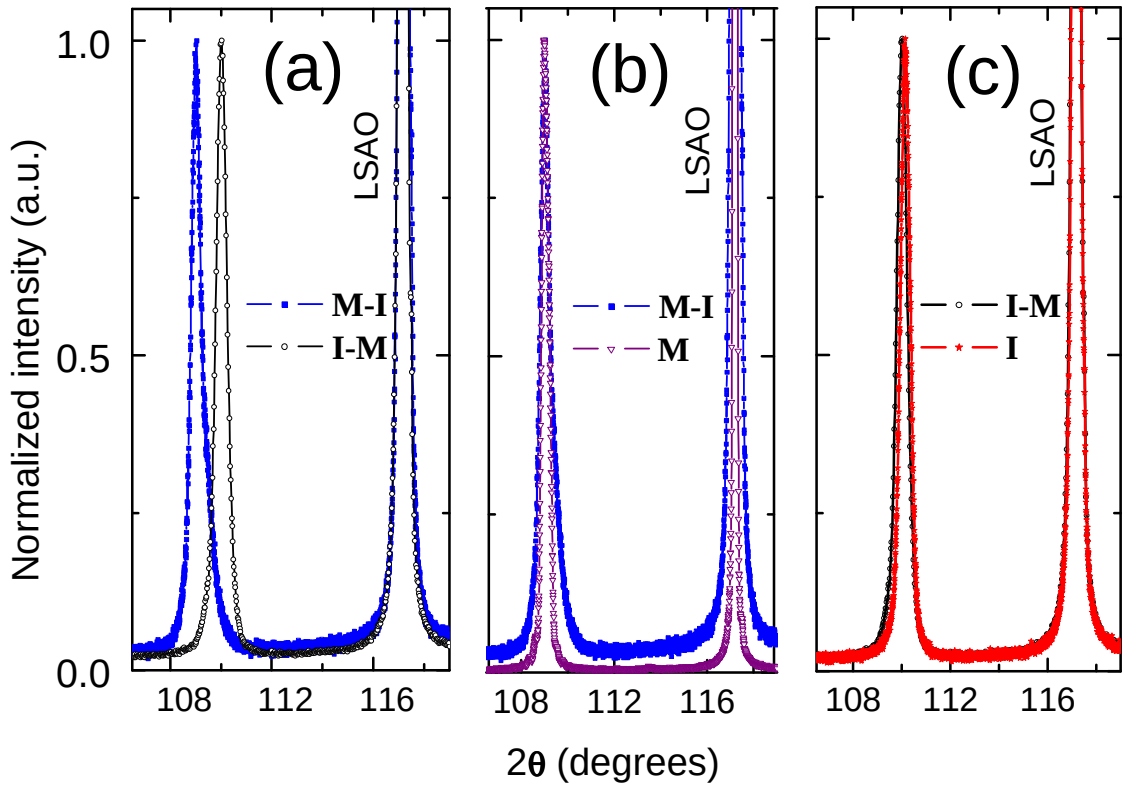

Figure 2. I-M and M-I bilayers have different structures, determined by the bottom layer. (a) A high-angle portion of the X-ray diffraction pattern (ω-2θ scan) of M-I and I-M bilayers grown on LSAO substrate, showing that the two structures have clearly distinct c_0 lattice constants. (b) The same for an M-I bilayer and a single-phase M film, showing that the two structures have essentially the same c_0 lattice constants. (c) The same for an I-M bilayer and a single-phase I film. The symbols I, M, and LSAO are defined in the caption to Table I.

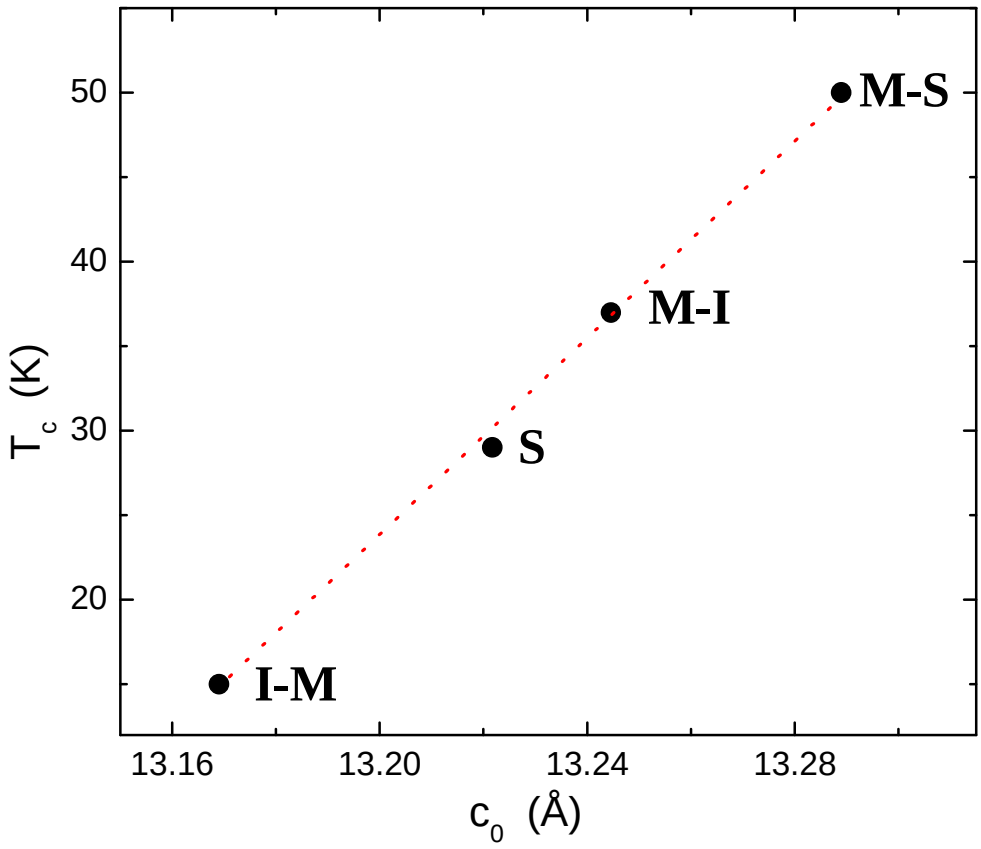

Figure 3. The dependence of the superconducting critical temperature, T_c, on the value of c_0 lattice constant in various La-Sr-Cu-O samples studied in this work. The symbols I, M, and S are defined in the caption to Table I. The values of T_c shown for I-M, M-I and M-S structures come from a very thin interfacial layer. Note that T_c also strongly depends on the hole density, which in the S layers within the M-S structures need not be the same as in our single-phase S films, because the c-axis expansion may affect the intake of interstitial oxygen. The dashed red line is a linear fit to the data.

Sample	a_0 (Å)	b_0 (Å)	c_0 (Å)	V (Å^3)
M layer	5.3137	5.3130	13.2451	373.934
M-I bilayer	5.3130	5.3122	13.2446	373.806
I layer	5.3751	5.3706	13.1545	379.742
I-M bilayer	5.3669	5.3618	13.169	378.960
S layer	5.3765	5.3745	13.2217	382.060
M-S bilayer	5.3113	5.3113	13.2890	374.894
I bulk[11]	5.4004	5.3574	13.1555	380.662
S bulk[30]	5.3346	5.3969	13.1646	379.019
LSAO	3.7564 (5.3123)	3.7564 (5.3123)	12.6357	178.297 (356.594)

Table 1. The values of lattice constants determined via the Nelson-Riley fitting procedure [29] from multiple Bragg peaks in X-ray diffraction patterns (ω-2θ scans), for various films grown on $LaSrAlO_4$ (LSAO) substrates. Here, M = $La_{1.56}Sr_{0.44}CuO_4$, a non-superconducting metal; I = La_2CuO_4, an antiferromagnetic insulator. M-I and I-M are bilayers in which each layer is 20 unit cells (26 nm) thick and oriented with CuO_2 planes parallel to the surface; the first letter denotes the layer next to the substrate. Note that every bilayer shows a single value of a_0, b_0, and c_0 lattice constants. For comparison, the data are also shown for I and for S = $La_2CuO_{4+\delta}$ bulk crystals [11,30] as well as for LSAO substrate. [To facilitate comparison, in parentheses we give the values for the unit cell doubled and rotated by 45^0.] Single-phase M has not been synthesized in bulk form.

Supplementary Information for "Madelung Strain in Cuprate Superconductors – A Route to Enhancement of the Critical Temperature" by V. Y. Butko, G. Logvenov, N. Bozovic, Z. Radovic and I. Bozovic*

In Figure S1, we show a photograph of the oxide molecular-beam epitaxy (MBE) system at BNL. A representative RHEED diffractogram obtained during growth of a La_2CuO_4 film is shown in Figure S2, the corresponding RHEED oscillation patterns in Figures S3 and S4. In Figure S5 we show a typical AFM image of the surface of such a film, showing rms surface roughness of no more than few Ångstroms. In Figure S6 we show the temperature dependence of resistivity data for single-phase I, M, and S films, and in Figure S7 the magnetic susceptibility data for I-M, M-I, and M-S bilayers, respectively, measured by the mutual inductance technique.

Figures 8-17 display X-ray data taken from various single-phase and bilayer films under study. The diffractograms demonstrate excellent epitaxial quality of the films. One can see from typical 2θ-ω scans for I, M, S, I-M, M-I, and M-S samples (Figures S8-S13, respectively) that all the (0, 0, L) diffraction peaks, with L = 2, 4, 6, 8, 10, 12 and 14, from the film and from the substrate are well resolved and that there are no peaks indicative of secondary-phase precipitates. The finite thickness fringes observed in Figures S14 and S15 are an indication of exceptional smoothness of the film surface. The angular distance between these fringes is consistent with the nominal thicknesses of the deposited film. The typical rocking curves (Figure S16) are very sharp, with FWHM of $0.03\text{-}0.06^0$, indicative of very little mosaicity in the films. A 3-dimensional image of X-ray diffraction intensity from a typical M-I sample measured in the 2-dimensional $2\theta/\omega$ - ω scan is presented in Figure S17. It shows that there is no peak of intensity in the reciprocal space region where one would expect to see a diffraction maximum from a bulk I layer (at $2\theta \sim 110^0$).

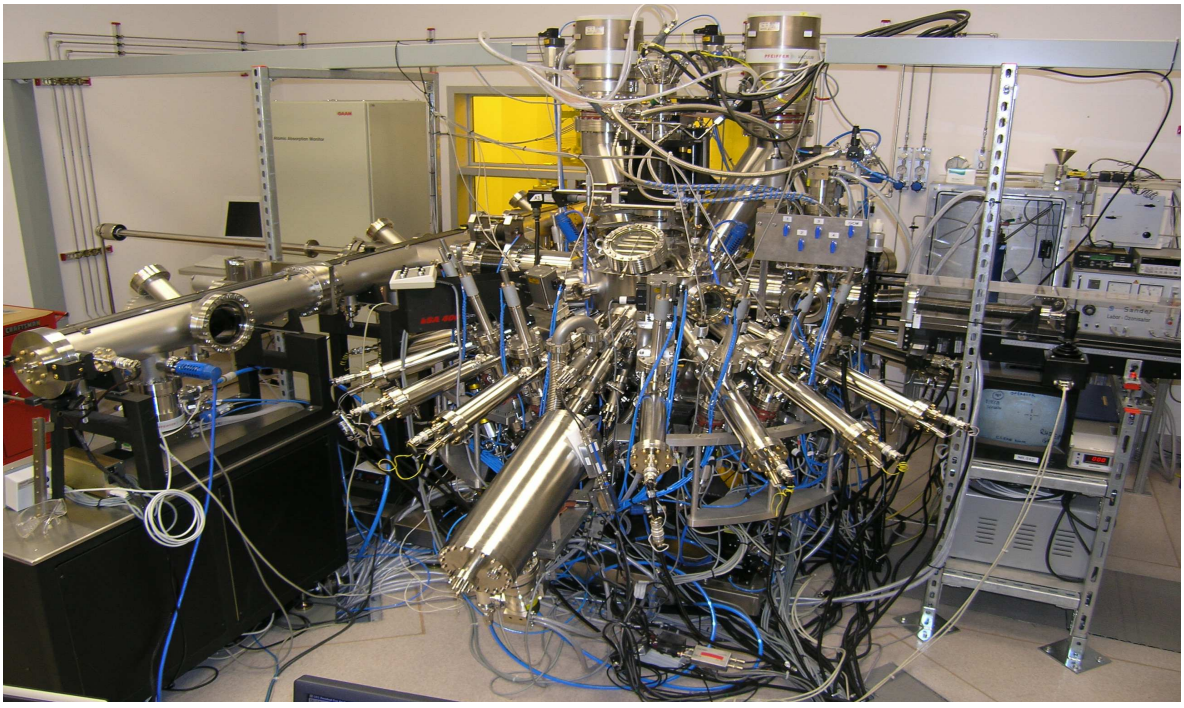

Supplementary Figure S1. The atomic-layer-by-layer molecular beam epitaxy (ALL-MBE) system at Brookhaven National Laboratory. It enables synthesis of thin films and multilayers of cuprate superconductors with atomically smooth surfaces and interfaces, and allows for the digital control of the layer thickness.

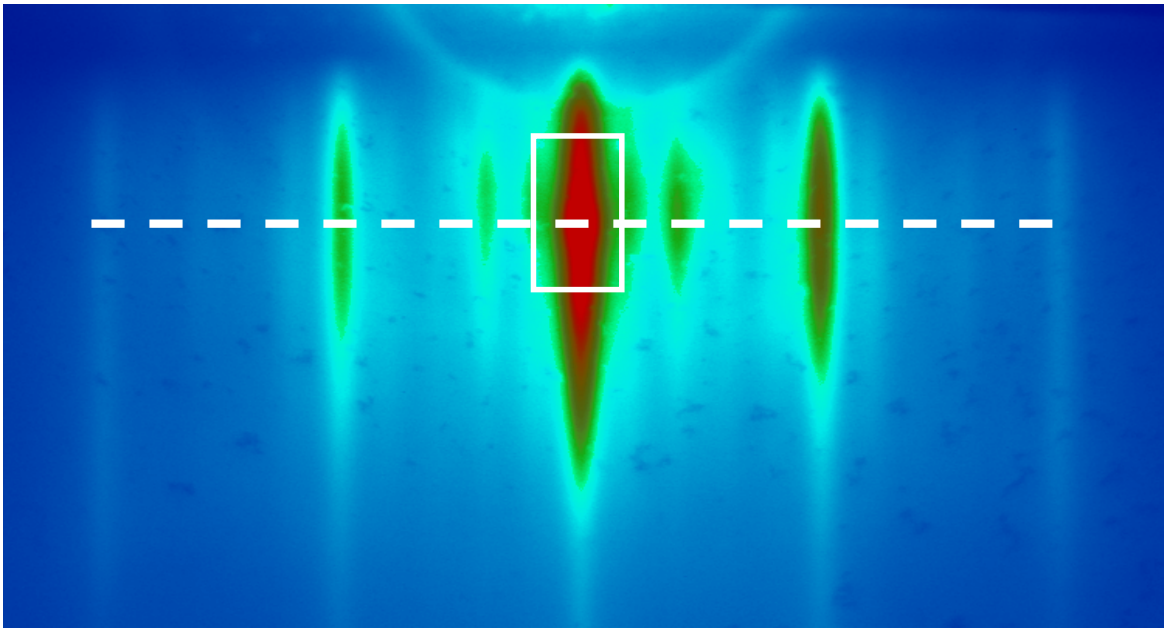

Supplementary Figure S2. RHEED pattern during growth of La_2CuO_4 layer. The intensity is color-coded for better visibility. The electron beam is nearly parallel to the (100) direction. The spacing between the major streaks corresponds to the in-plane lattice spacing a_0 = 3.8 A. Four weaker side-bands are visible between each pair of main diffraction streaks, indicating some surface reconstruction with five time larger lattice spacing. The pattern changes periodically during deposition.

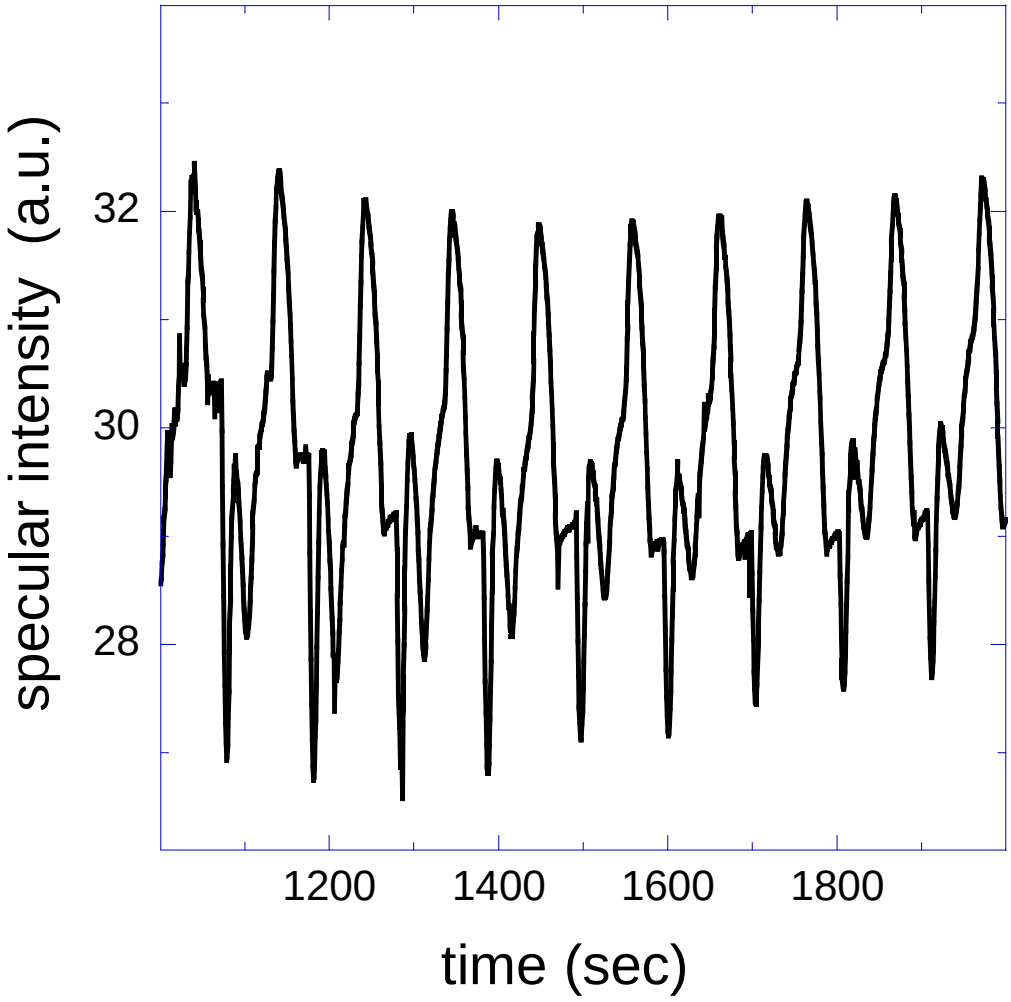

Supplementary Figure S3. The time-dependence of the intensity of specular RHEED reflection (integrated over the area indicated by the white square in Figure S2), during growth of a La_2CuO_4 film.

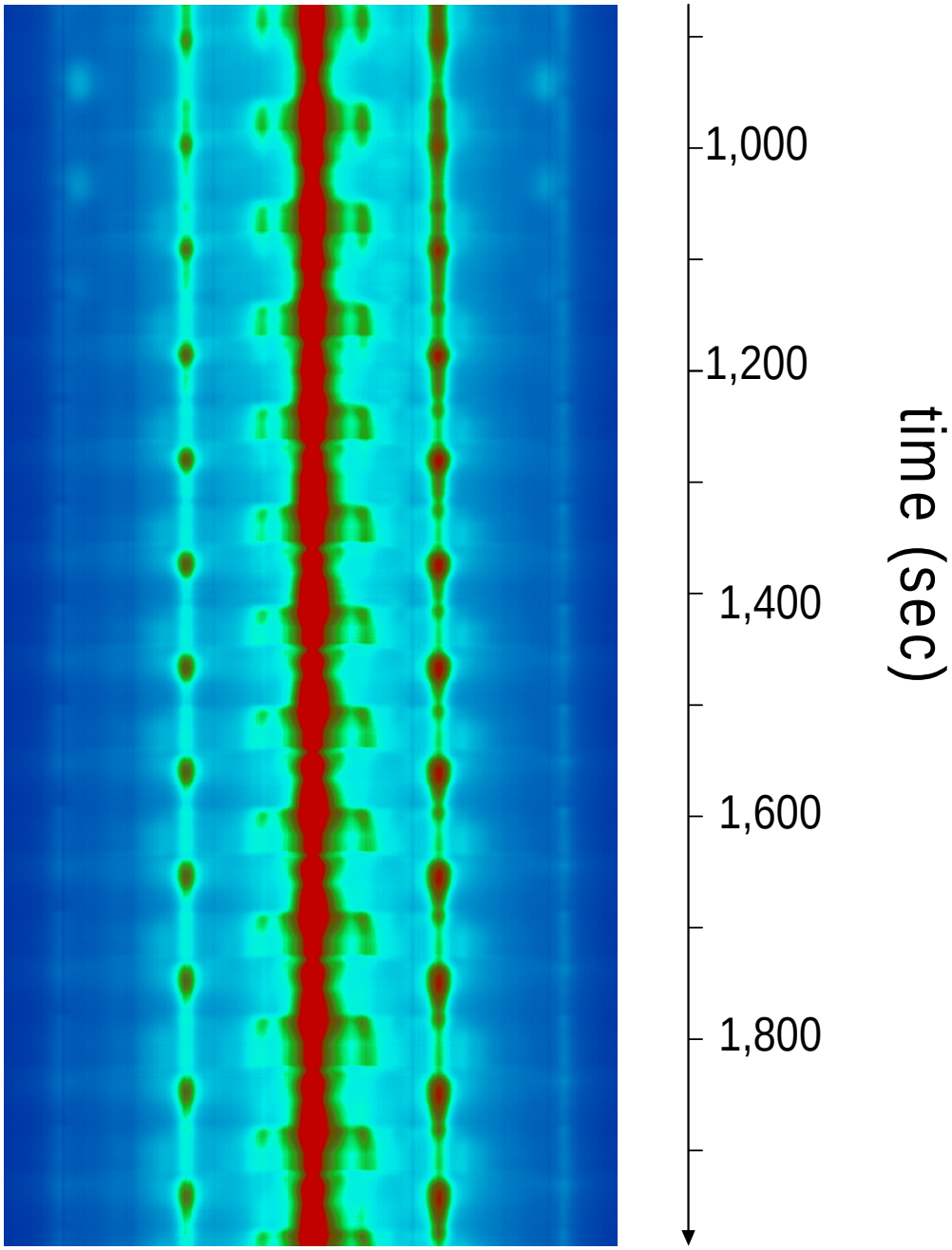

Supplementary Figure S4. The time-dependence of RHEED intensity as a function of position along the dashed white line shown in Figure S2, during growth of a La_2CuO_4 film. The intensity is color-coded the same way as in Figure S2. The time-flow arrow is downwards.

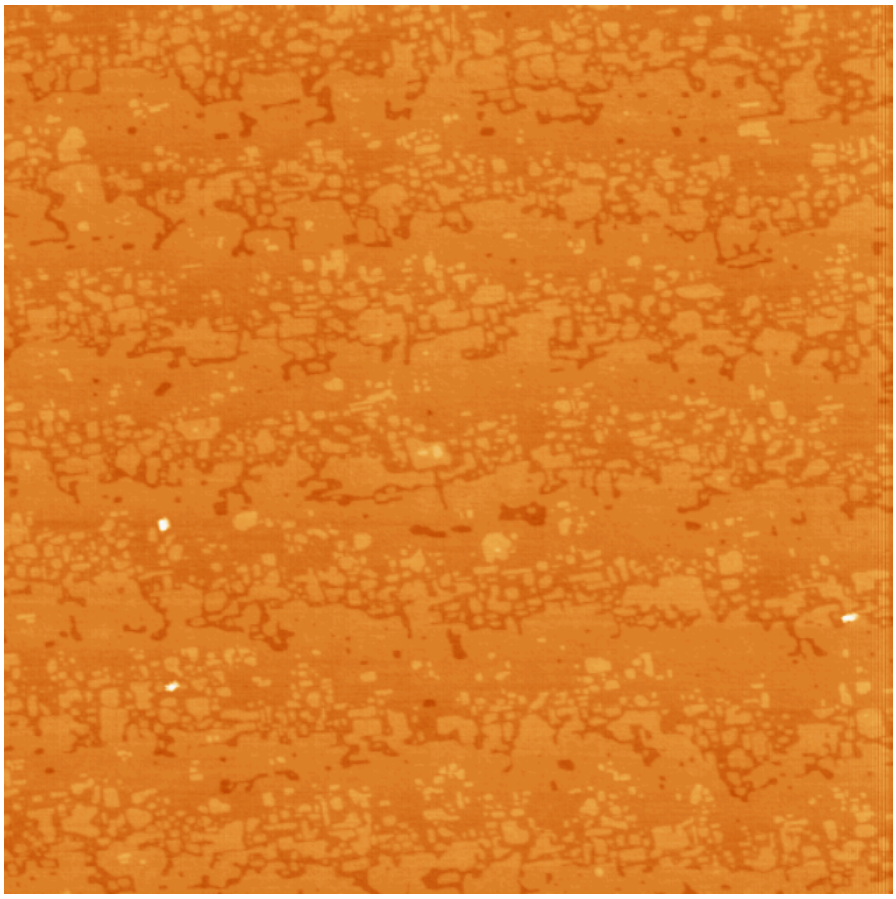

Supplementary Figure 5. A typical Atomic Force Microscopy image of an M-I film on LSAO substrate. It shows rms surface roughness of 0.29 nm over a large area of 25 μm^2. Other films studied in the present work have shown similar surface quality.

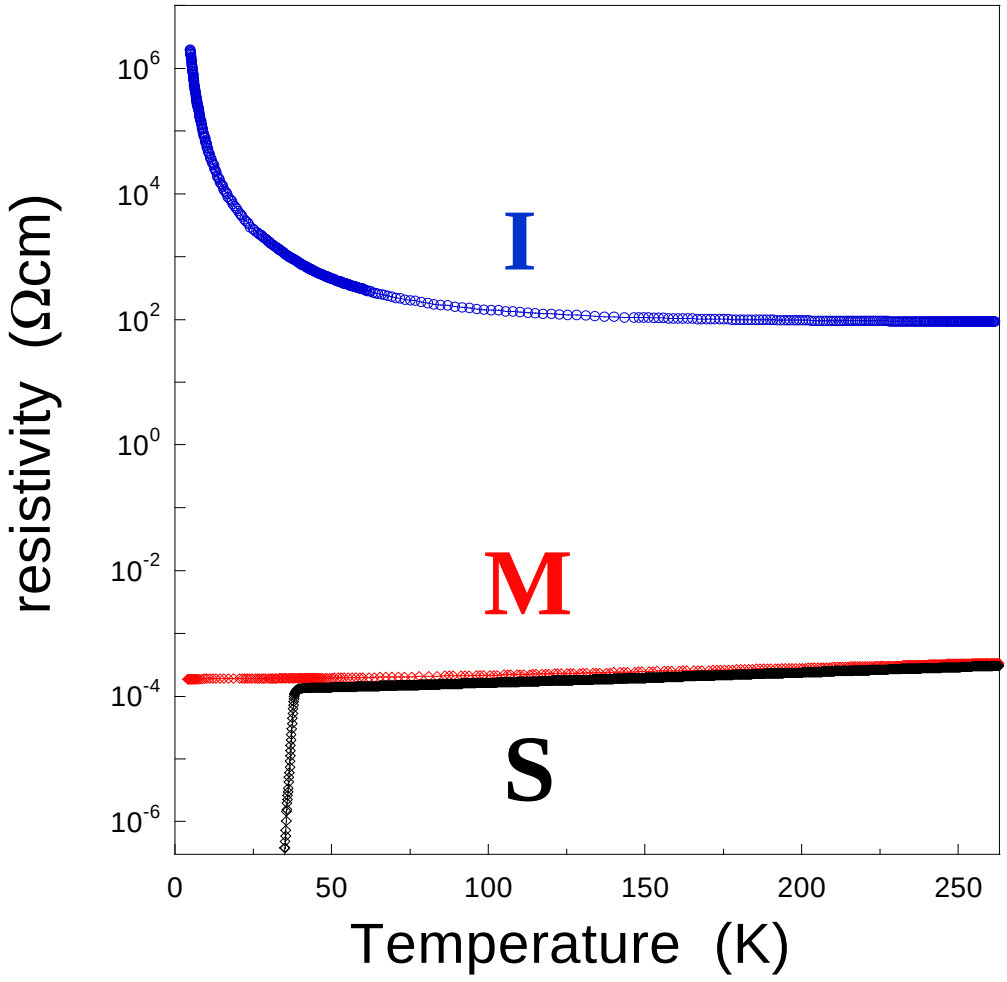

Supplementary Figure 6. Resistivity vs. temperature data for typical I = La_2CuO_4, M = $La_{1.55}Sr_{0.45}CuO_4$, and S = $La_2CuO_{4+\delta}$ films.

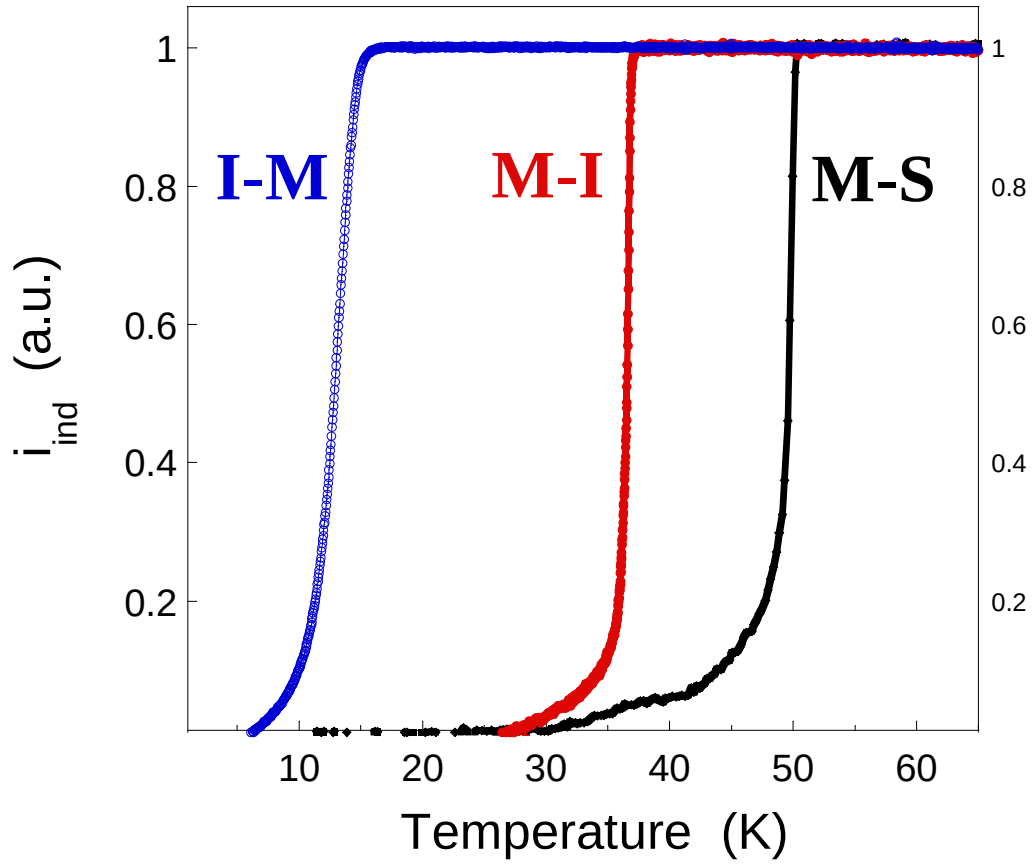

Supplementary Figure 7. Mutual inductance vs. temperature data for typical I-M, M-I, and M-S bilayers, showing T_c ≈15 K, T_c ≈ 36 K and T_c ≈ 51 K, respectively. Here, i_{ind} is the out-of-phase (reactive) component of the current induced in the pick-up coil, placed on the opposite side of the film from the drive coil; it is determined by the drive coil current and the geometry (which are the same for all three samples), and the magnetic susceptibility of the film.

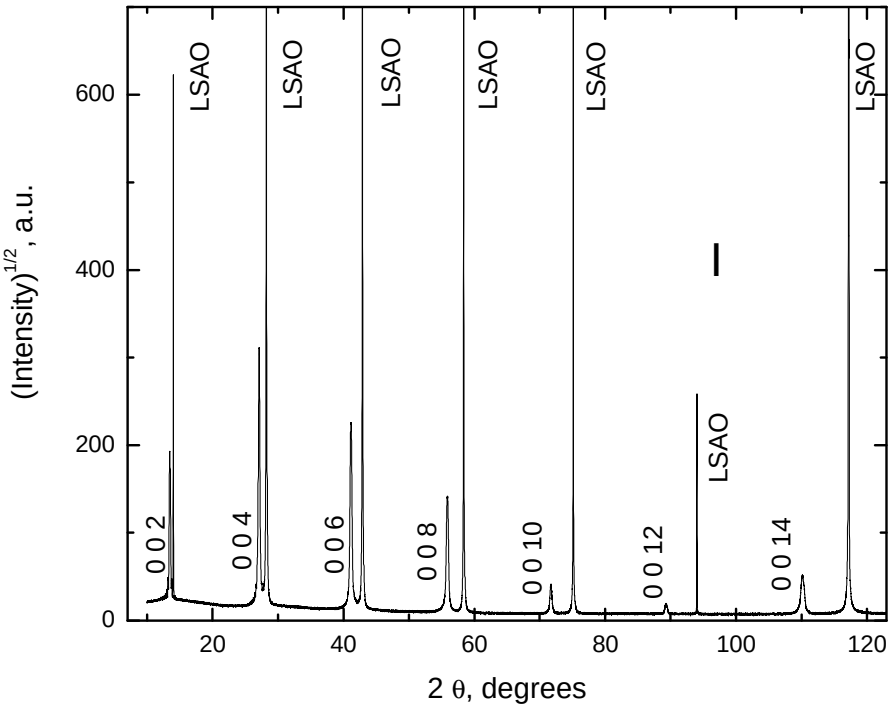

Supplementary Figure 8. X-ray diffraction of an I film on LSAO substrate: 2Θ–ω scan taken over a large angle range. The film is 40 UC (52 nm) thick. The diffractogram shows sharp (0, 0, L) peaks with L = 2, 4, ..., 14, of both the film and the substrate. No other peaks, such as would originate from secondary phase precipitates, are detectable. The same is true of all other samples studied here (Figures S9-S15).

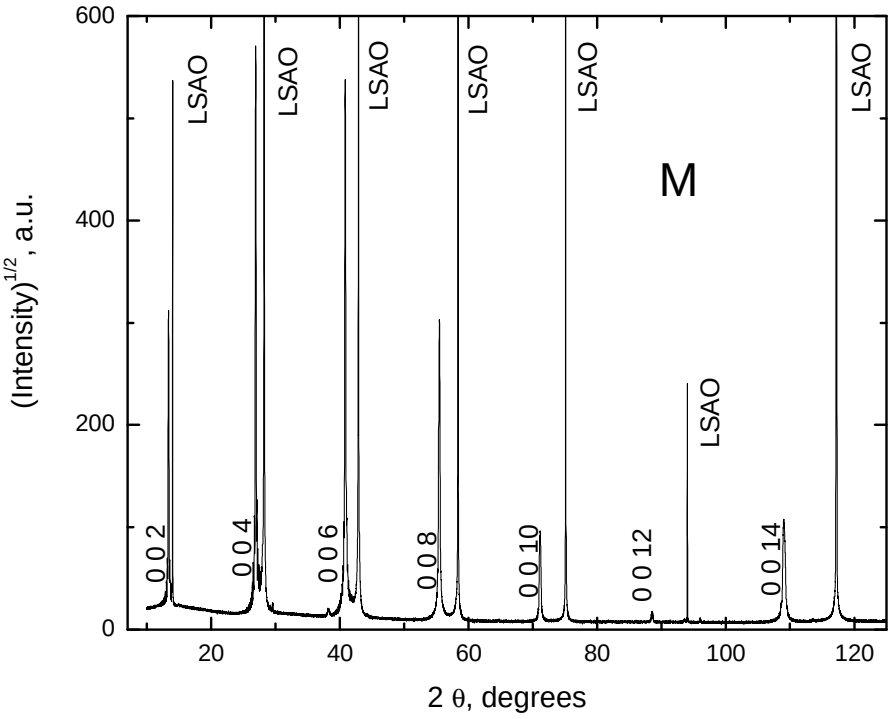

Supplementary Figure 9. X-ray diffraction of an M film on LSAO substrate: 2Θ–ω scan taken over a large angle range. The film is 40 UC (52 nm) thick.

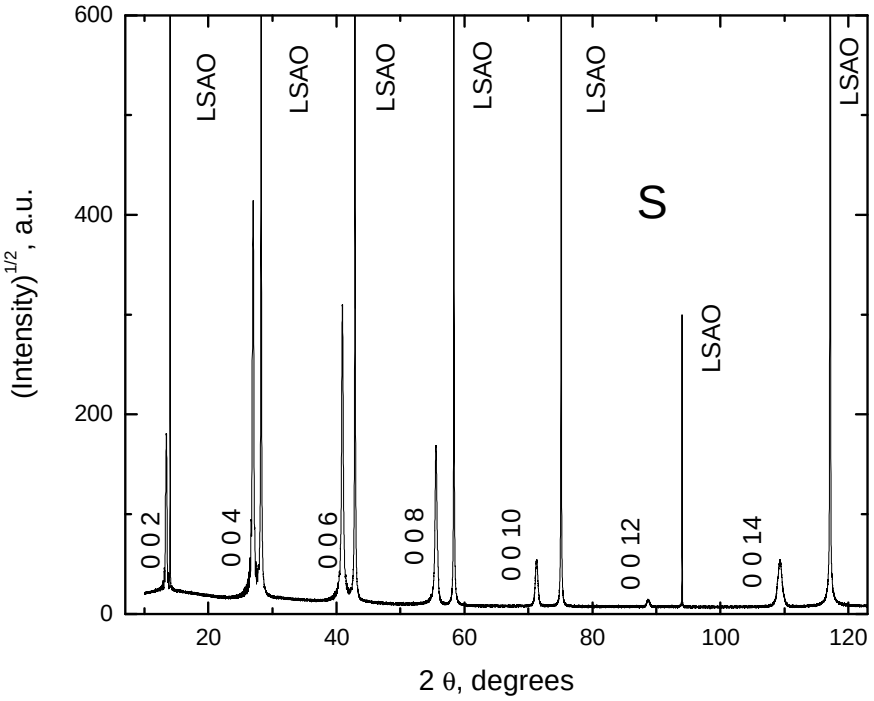

Supplementary Figure 10. X-ray diffraction of an S film on LSAO substrate: 2Θ–ω scan taken over a large angle range. The film is 40 UC (52 nm) thick.

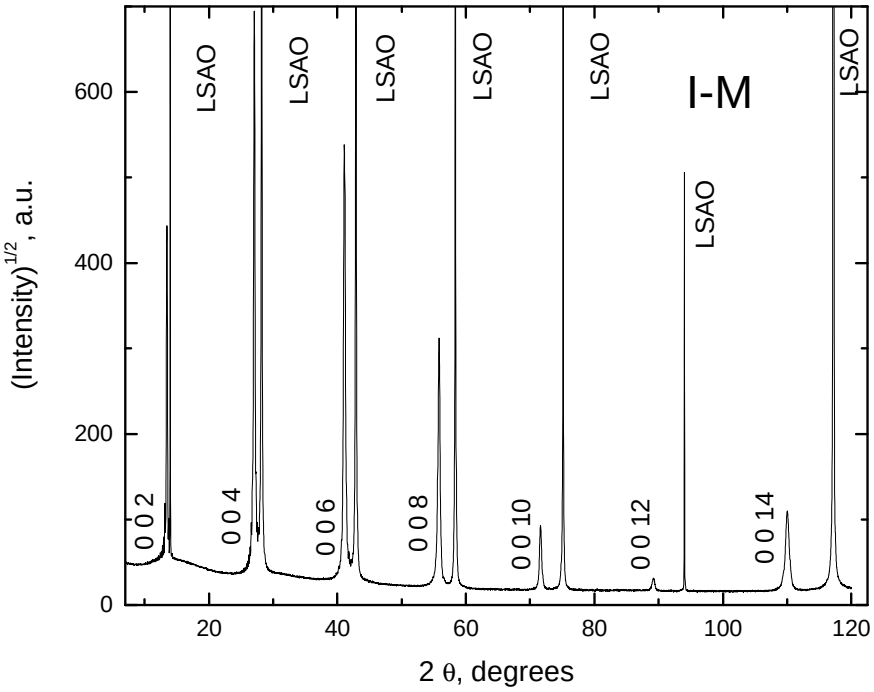

Supplementary Figure 11. X-ray diffraction of an I-M bilayer film on LSAO substrate: 2Θ–ω scan taken over a large angle range. Each of the two layers is 20 UC (26 nm) thick.

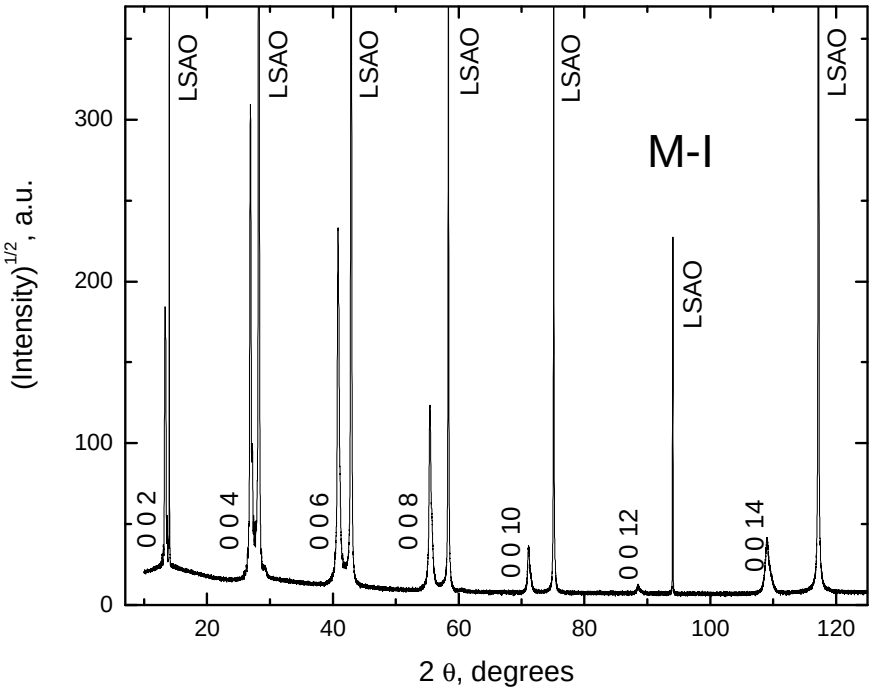

Supplementary Figure 12. X-ray diffraction of an M-I bilayer film on LSAO substrate: 2Θ–ω scan taken over a large angle range. Each layer is 20 UC (26 nm) thick.

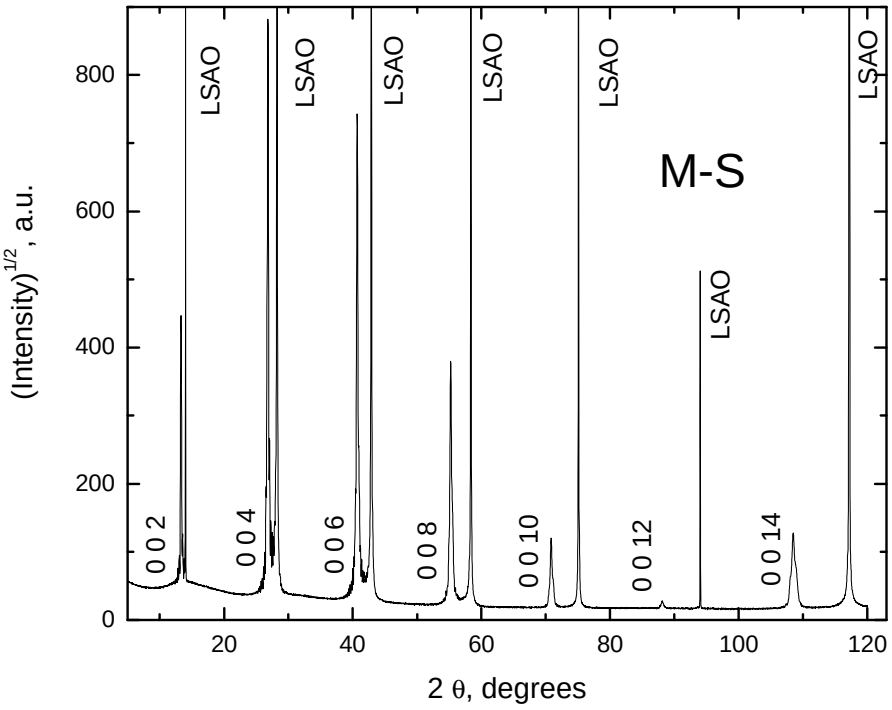

Supplementary Figure 13. X-ray diffraction of an M-S bilayer film on LSAO substrate: 2Θ–ω scan taken over a large angle range. Each layer is 20 UC (26 nm) thick.

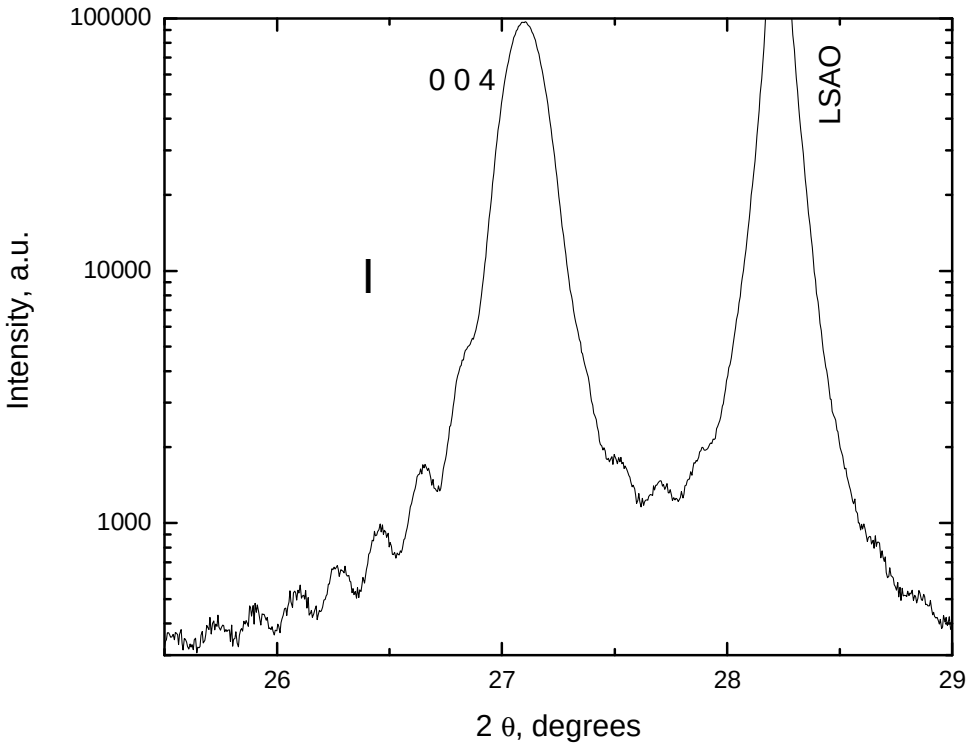

Supplementary Figure 14. X-ray diffraction of an I film on LSAO substrate: 2Θ–ω scan taken near the (0,0,4) Bragg reflection. It shows pronounced finite-thickness oscillations, evidencing of the atomically smooth film surface and substrate/film interface.

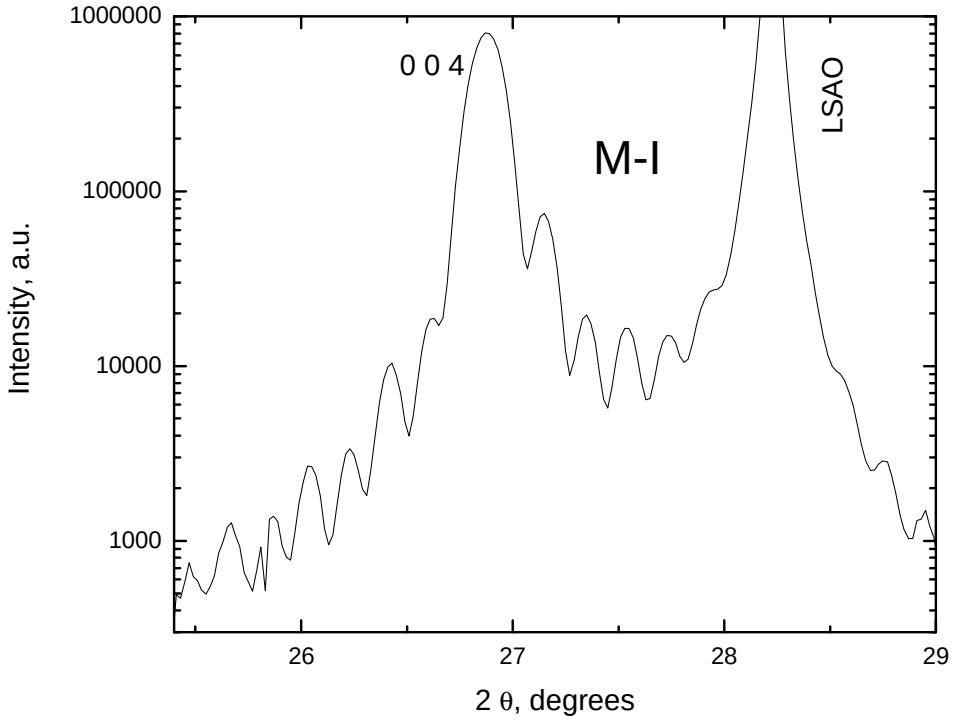

Supplementary Figure 15. X-ray diffraction: 2Θ–ω scan taken near the (0,0,4) Bragg reflection of an M-I bilayer film on LSAO substrate. It shows pronounced finite-thickness oscillations, evidencing of the atomically smooth film surface and substrate/film interface.

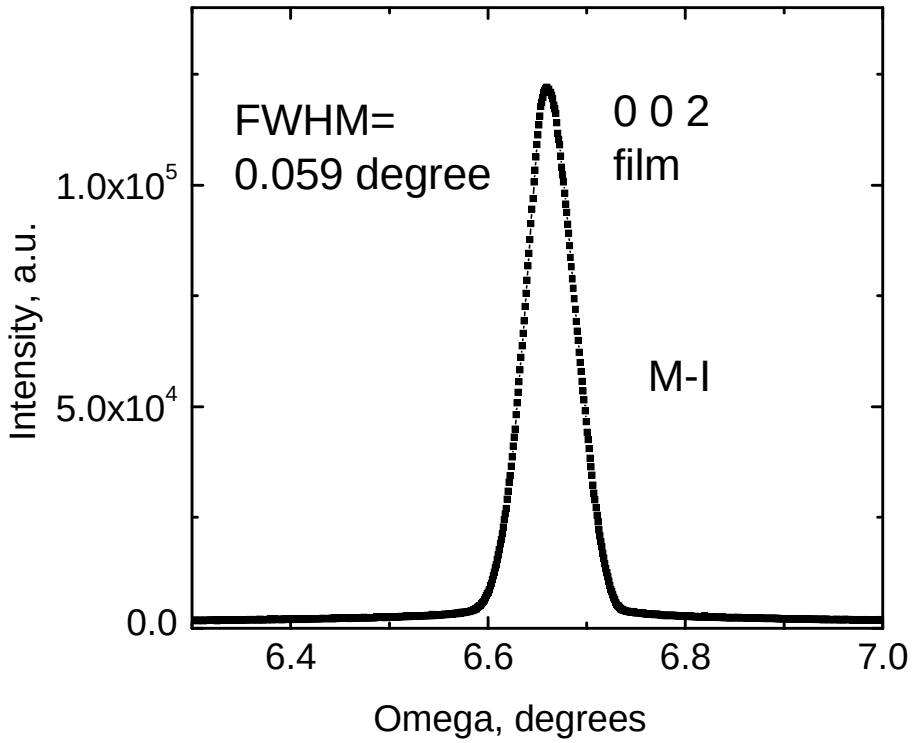

Supplementary Figure 16. X-ray diffraction: the ω-rocking curve taken near the (0,0,2) Bragg reflection of an M-I bilayer film on LSAO substrate. The full width at the half maximum (FWHM) is very small, less then 0.06^0, which is comparable to that of the LSAO substrate itself. It indicates that there is very little mosaicity in the film.

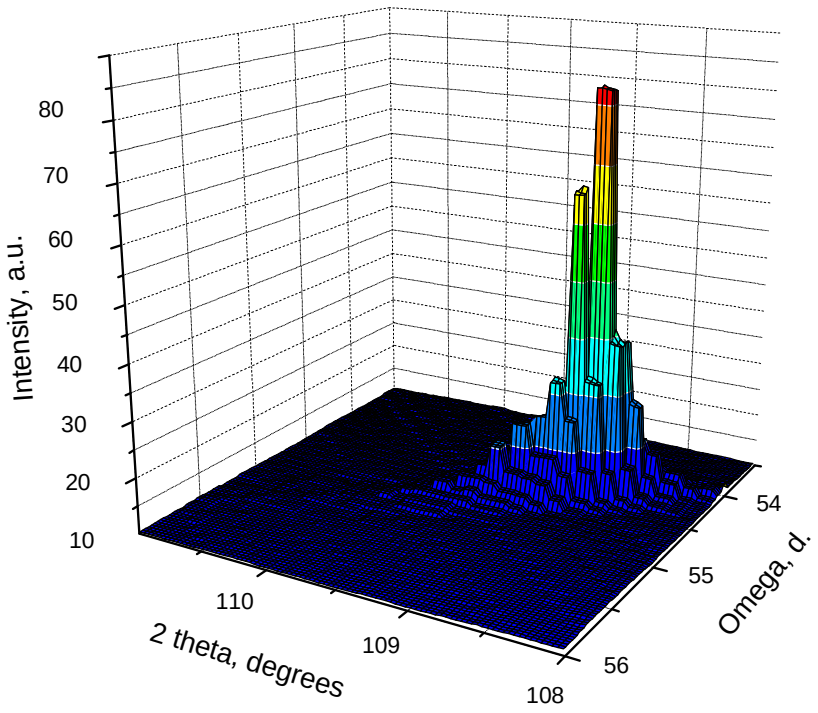

Supplementary Figure 17. X-ray diffraction: the 2-dimensional scan, 2Θ–ω vs ω, taken near the (0,0,14) Bragg reflection of an M-I bilayer film on LSAO substrate. It shows that there is only a single peak; there is no large peak splitting (~1^0) such as would be expected if each of the two layers retained their nominal bulk structure. [See the simulated patterns in Figures 1c and 1d in the main text.]